Chinese Journal of Natural Medicines

Andrographolide sulfonate alleviates rheumatoid arthritis by inhibiting glycolysis-mediated activation of PI3K/AKT to restrain Th17 cell differentiation

Chunhong Jiang, Xi Zeng, Jia Wang, Xiaoqian Wu, Lijuan Song, Ling Yang, Ze Li, Ning Xie, Xiaomei Yuan, Zhifeng Wei, Yi Guan

Citation: Chunhong Jiang, Xi Zeng, Jia Wang, Xiaoqian Wu, Lijuan Song, Ling Yang, Ze Li, Ning Xie, Xiaomei Yuan, Zhifeng Wei, Yi Guan, Andrographolide sulfonate alleviates rheumatoid arthritis by inhibiting glycolysis-mediated activation of PI3K/AKT to restrain Th17 cell differentiation, Chinese Journal of Natural Medicines, 2025, 23(4), 480-491. doi: 10.1016/S1875-5364(25)60855-7.

View online: https://doi.org/10.1016/S1875-5364(25)60855-7

Chinese Journal of Natural Medicines 23 (2025) 480-491

Contents lists available at ScienceDirect

Chinese Journal of Natural Medicines

journal homepage: www.cjnmcpu.com/

Original article

Andrographolide sulfonate alleviates rheumatoid arthritis by inhibiting glycolysis-mediated activation of PI3K/AKT to restrain Th17 cell differentiation

Chunhong Jiang[a], Xi Zeng[b], Jia Wang[a], Xiaoqian Wu[b], Lijuan Song[b], Ling Yang[b], Ze Li[b], Ning Xie[c], Xiaomei Yuan[a], Zhifeng Wei[b,*], Yi Guan[a,d,*]

[a] *Guangdong-Hong Kong Joint Laboratory for Emerging Infectious Diseases, Joint Institute of Virology (Shantou University and The University of Hong Kong), Shantou University Medical College, Shantou 515041, China*

[b] *Department of Pharmacology of Chinese Materia Medica, China Pharmaceutical University, Nanjing 210009, China*

[c] *State Key Laboratory of Innovative Natural Medicine and TCM Injection, Ganzhou 341000, China*

[d] *State Key Laboratory of Emerging Infectious Diseases (SKLEID), School of Public Health, Li Ka Shing Faculty of Medicine, The University of Hong Kong, Hong Kong SAR, China*

ARTICLE INFO

Article history:
Received 26 February 2024
Revised 13 May 2024
Accepted 28 May 2024
Available online 20 April 2025

Keywords:
Andrographolide sulfonate
Rheumatoid arthritis
Th17 cell differentiation
Glycolysis
PI3K/AKT pathway

ABSTRACT

Andrographolide sulfonate (AS) is a sulfonated derivative of andrographolide extracted from *Andrographis paniculata* (Burm.f.) Nees, and has been approved for several decades in China. The present study aimed to investigate the novel therapeutic application and possible mechanisms of AS in the treatment of rheumatoid arthritis. Results indicated that administration of AS by injection or gavage significantly reduced the paw swelling, improved body weights, and attenuated pathological changes in joints of rats with adjuvant-induced arthritis. Additionally, the levels of tumor necrosis factor-alpha (TNF-α), interleukin-6 (IL-6), and IL-1β in the serum and ankle joints were reduced. Bioinformatics analysis, along with the spleen index and measurements of IL-17 and IL-10 levels, suggested a potential relationship between AS and Th17 cells under arthritic conditions. *In vitro*, AS was shown to block Th17 cell differentiation, as evidenced by the reduced percentages of $CD4^+$ $IL\text{-}17A^+$ T cells and decreased expression levels of RORγt, IL-17A, IL-17F, IL-21, and IL-22, without affecting the cell viability and apoptosis. This effect was attributed to the limited glycolysis, as indicated by metabolomics analysis, reduced glucose uptake, and pH measurements. Further investigation revealed that AS might bind to hexokinase2 (HK2) to down-regulate the protein levels of HK2 but not glyceraldehyde-3-phosphate dehydrogenase (GAPDH) or pyruvate kinase M2 (PKM2), and overexpression of HK2 reversed the inhibition of AS on Th17 cell differentiation. Furthermore, AS impaired the activation of phosphatidylinositol 3-kinase (PI3K)/protein kinase B (AKT) signals *in vivo* and *in vitro*, which was abolished by the addition of lactate. In conclusion, AS significantly improved adjuvant-induced arthritis (AIA) in rats by inhibiting glycolysis-mediated activation of PI3K/AKT to restrain Th17 cell differentiation.

1. Introduction

Rheumatoid arthritis (RA) is a prevalent autoimmune disorder, characterized by chronic inflammation, joint swelling, and symmetrical progressive polyarticular destruction [1]. As the disease progresses, approximately half of RA patients experience extra-articular symptoms, affecting multiple tissues and organs such as the heart, kidney, lung, skin, eyes, nerves, and gastrointestinal tract. Epidemiological studies indicate that the global incidence of RA ranges from 0.5% to 1%, predominantly affecting middle-aged and elderly individuals, with a significantly higher prevalence in women compared to men, at a ratio of approximately 3∶1 [2, 3]. Repeated episodes, prolonged illness, and a significant decline in physical function, quality of life, and work capacity impose a considerable burden on patients, their families, and society as a whole [4].

The drugs used in clinical for RA mainly include non-steroidal anti-inflammatory drugs (NSAID), steroids, disease-modifying anti-rheumatic drugs (DMARDs), and biologics. However, these treatments frequently produce a substantial number of adverse effects, such as retinopathy and impaired liver and kidney function [5, 6]. Additionally, some drugs have a short half-life or insufficient concentration at the lesion site, necessitating higher doses and more frequent administration, which can lead to severe side effects and increased treatment costs. In cases of significant joint damage or treatment failure, patients may require surgical intervention, though the postoperative outcomes are often unsatisfactory [7]. Therefore, there is a pressing need to identify new, safe, and effective pharmacotherapies for RA, as well as to develop optimal treatment regimens.

The major constituent of *Andrographis paniculata* (Burm.f.) Nees, andrographolide, has exhibited anti-arthritic effects in addition to anti-inflammatory, anti-infective, and anticancer properties [8]. However, the extremely low water solubility has greatly limited its clinical application [9]. The soluble andrographolide de-

* Corresponding author.
E-mail addresses: 1020132346@cpu.edu.cn (Z. Wei); yguan@hku.hk (Y. Guan)

https://doi.org/10.1016/S1875-5364(25)60855-7

rivative, andrographolide sulfonate (AS), is approved for the treatment of bronchitis, tonsillitis, and bacillary dysentery. It is reported that AS can improve the survival rate and attenuate the liver and lung injury of lipopolysaccharide-induced septic mice [10]. The clinical symptoms, such as diarrhea and colon shortening of colitis mice, are also alleviated by AS [11]. It is noteworthy that the existing studies on the pharmacological effects of AS have primarily focused on diseases in the respiratory and digestive systems, while research into the effect of AS on RA has not yet been reported. Based on bioinformatics analysis, we initially identified a potential relationship between AS and RA. This study is designed to investigate the therapeutic effects of AS on RA and further elucidate the underlying molecular mechanisms.

2. Materials and Methods

2.1. Drugs and reagents

AS (Batch No. 20210119) was provided by Jiangxi Qingfeng Pharmaceutical Co., Ltd., a company based in Ganzhou. Dexamethasone acetate tablets (DEX, Catalog No. 015191012) were purchased from Shanghai Sine Pharmaceutical Laboratories (Shanghai, China). Desiccated *Mycobacterium butyricum* was provided by Becton, Dickinson and Company (Franklin Lakes, NJ, USA); Anhydrous lanolin (CAS No. 8006-54-0) was purchased from Rhawn Reagent (Shanghai, China); Hematoxylin and eosin staining solution was purchased from BaSO Biotechnology (Wuhan, China); NP-40 lysis buffer and BCECF-AM were purchased from Shanghai Beyotime Biotechnology (Shanghai, China). Thermo Fisher Scientific (Waltham, MA, USA) provided the rat tumor necrosis factor-alpha (TNF-α) enzyme-linked immunosorbent assay (ELISA) kit, while the Yi Fei Xue Biotechnology (Nanjing, China) supplied the rat interleukin-6 (IL-6), IL-1β, IL-10, and IL-17 ELISA kits. Sangon Biotech (Shanghai, China) and Shanghai Beyotime Biotechnology (Shanghai, China) supplied antibodies against phosphatidylinositol 3-kinase (PI3K), protein kinase B (AKT), phosphorylated AKT (p-AKT), and p-PI3K. Nanjing Biogot Technology (Nanjing, China) provided antibodies against RORγt and *β*-actin. Abclonal (Wuhan, China), Wanleibio (Shenyang, China), and Proteintech (Wuhan, China) provided antibodies against hexokinase2 (HK2), pyruvate kinase M2 (PKM2), and glyceraldehyde-3-phosphate dehydrogenase (GAPDH), respectively. PeproTech (Madison, USA) supplied TGF-β, IL-6, and IL-23 recombinant protein. Mixtures of PMA/ionomycin and BFA/monensin were obtained from Multisciences (Lianke) (Hangzhou, China). Antibodies against CD3/CD28, anti-IL-17A-APC, and anti-CD4-FITC were obtained from Thermo Fisher Scientific (San Diego, USA). HK2 plasmid for overexpression was purchased from Genomeditech (Shanghai, China). PEI 40K Transfection agent was obtained from Servicebio (Wuhan, China). 2-NBDG was purchased from Invitrogen Corp. (Carlsbad, USA). TRIzol reagent and HiScript Q RT Super Mix were purchased from Vazyme (Nanjing, China); Polyvinylidene fluoride (PVDF) membrane was purchased from Millipore Sigma (Burlington, MA, USA).

2.2. Animals

Female Wistar rats, weighing 130−150 g, were obtained from Charles River Laboratories Co., Ltd. [laboratory animal production license number: SCXK (Zhejiang) 2021-0006; Wilmington, MA, USA]. The rats were housed under specific pathogen-free (SPF) conditions, provided ad libitum access to food and water, and acclimated for 3 days prior to experimentation. All animal experiments were approved by the Animal Ethics Committee of China Pharmaceutical University (approval No. 2021-11-010) and conducted in strict accordance with guidelines issued by the committee.

2.3. Establishment of AIA model in rats and drug treatment

The AIA model was established using previously reported methods [12, 13] with minor modifications. Anhydrous lanolin was melted by heating, and liquid paraffin was added. The mixture was combined with desiccated *Mycobacterium butyricum* at a ratio of 1 mL/10 mg to prepare Freund's complete adjuvant, which was then intradermally injected into the right hind paws and tail roots of the rats.

On day 14 after immunization, the AIA rats were randomly divided into seven groups (n = 6/group) based on the degree of secondary paw swelling: model group, AS groups (25, 50, and 100 mg·kg^{-1} administered by tail vein injection, and 100 and 200 mg·kg^{-1} administered by gavage), and DEX group (0.5 mg·kg^{-1} administered by gavage). From day 14 to 27, rats in each group were administered with the corresponding dose once daily.

2.4. Measurement of paw swelling and arthritis index (AI) scores

During the experimental period, a rat plethysmometer (ZH-ZZY; Anhui Zhenghua Biologic Apparatus Facilities, Huaibei, China) was used to measure the volume of the left and right hind paws. In addition, the cumulative AI scores were calculated to evaluate the severity of arthritis based on the degree of swelling in the left hind paw and forelimbs, erythema behind the ears, and the presence of nodules in the tail.

2.5. Measurement of body weights and splenic indexes

After the final administration, the rats were sacrificed, and their spleens were extracted. The spleens were then immediately washed, excess liquid was removed from their surfaces, and they were weighed. The splenic index was calculated using the formula: Splenic index = Spleen weight (mg)/Body weight (g).

2.6. Imaging analysis

Following the final administration, the bilateral paws of the rats were photographed using a mini single-lens reflex camera (Fujifilm XT-200; Tokyo, Japan). The X-ray images of the bilateral ankle joints were acquired using a small animal X-ray digital imaging system (MX-20; Faxitron, Tucson, AZ, USA).

2.7. Histopathological analysis

The ankle joint specimens were collected, fixed in a 4% polyformaldehyde solution, decalcified using ethylenediaminetetraacetic acid (EDTA), dehydrated, embedded in paraffin, and sectioned. Subsequently, the sections were stained with hematoxylin and eosin (H&E) and examined under an optical microscope (IX53; Olympus, Tokyo, Japan) to analyze the pathological changes.

The assessment of pathological changes and their scoring were conducted as follows: a. pathological changes [14]: (1) presence or absence of erosion (degeneration, necrosis) and hyperplasia in synovial cells; (2) presence or absence of inflammatory cell infiltration; (3) presence or absence of pannus (composed of blood vessels and fibroblasts); (4) presence or absence of bone erosion (destruction of articular bone and cartilage). b. Scoring: quantitative scores of 0−4 were assigned based on the severity of pathological changes in each area: 0 points, normal (no changes); 1 point, mild; 2 points, moderate; 3 points, severe; 4 points, extremely severe. The scores of all areas were summed up to calculate the total score for each rat.

2.8. Enzyme-linked immunosorbent assay (ELISA)

The concentrations of tumor necrosis factor-alpha (TNF-α),

IL-6, IL-1β, IL-17, and IL-10 in serum or joint tissues were quantified using ELISA kits in accordance with the manufacturer's protocol.

2.9. Relationship between AS and RA

We used 140 potential AS targets predicted in the previous study [15] for Genetic Association Database (GAD) disease analysis and Kyoto Encyclopedia of Genes and Genomes (KEGG) pathway enrichment analysis using the Database for Annotation, Visualization, and Integrated Discovery (DAVID) (https://david.ncifcrf.gov/tools.jsp). Notably, RA was identified in both disease association results (Supplementary Fig. S1). To identify potential disease-related genes, we queried the GeneCards database (https://www.genecards.org/) with the keyword "rheumatoid arthritis" and extracted RA-related genes with relevant scores >1. The intersection of AS and RA-related genes was then analyzed using the STRING (http://string-db.org/) construct protein-protein interaction (PPI) networks, with a minimum interaction score of 0.7. Cytoscape 3.9.2 software was used for visualizing PPIs, and CytoHubba, a new Cytoscape plugin for ranking node features in networks, was employed to identify hub genes. For enhanced visualization, node sizes were adjusted proportionally to the degree magnitude, and edge thickness was scaled according to the combined interaction score.

2.10. Cell viability and apoptosis

The cells were seeded in 96-well plates and incubated for 72 h, and 20 μL of a 5 mg·mL^{-1} MTT solution was applied to each well for 4 h. After incubation, 150 μL of dimethyl sulfoxide was added, and the media was removed. After the crystals had been dissolved completely, the absorbance value was measured at 570 nm.

The cells were harvested and then rinsed with phosphate buffer saline (PBS). Afterward, they were resuspended in 1 × binding buffer, and Annexin V-FITC and PI dyes were then added in accordance with the instructions of the Annexin V-FITC/PI apoptosis detection kit (Solarbio; Beijing, China). Finally, the percentage of apoptotic cells was determined by flow cytometry.

2.11. Western blotting analysis

Total protein was extracted using RIPA lysis buffer and quantified with a bicinchoninic acid (BCA) assay kit (P0012; Beyotime). Proteins of varying molecular weights were separated by 8% or 10% sodium dodecyl sulfate-polyacrylamide gel electrophoresis (SDS-PAGE) and transferred to a PVDF membrane. The membrane was blocked in 9% skim milk at room temperature for 2 h, and incubated overnight at 4 °C with primary antibodies. The corresponding secondary antibodies were applied at room temperature for 2 h. Subsequently, the enhanced chemiluminescence (ECL) reagent was selected to visualize the protein bands using a gel imaging system (Tanon 4600; Tanon Science & Technology, Shanghai, China). The grayscale values of bands were quantitatively analyzed using Image-Pro Plus (Media Cybernetics, Rockville, MD, USA).

2.12. $CD4^+$ $IL\text{-}17A^+$ (Th17) cell differentiation

Following separation, the mesenteric lymph nodes (MLNs) were crushed and passed through a 70 μm filter. The resulting filtrate was centrifuged, and the precipitate was collected, rinsed with phosphate-buffered saline (PBS), and resuspended in RPMI-1640 medium to obtain a lymphocyte suspension. This suspension was then subjected to the MojoSort™ mouse CD4 Naïve T cell isolation kit (480039, BioLegend, San Diego, USA) to extract $CD4^+$ T cells. The cells were seeded in 96-well plates pre-coated with anti-CD3 (1 μg·mL^{-1}) and supplemented with anti-CD28 (1 μg·mL^{-1}), TGF-β (2 ng·mL^{-1}), IL-6 (40 ng·mL^{-1}), IL-23 (10 ng·mL^{-1}) at 37 °C for 72 h. Following the incubation, fluorescence labeling, and flow cytometry analysis were performed.

2.13. Th17 cell ratio determination

Differentiated lymphocytes were collected and stimulated with a PMA/Ionomycin mixture and a BFA/Monensin mixture, followed by incubation for 5 h at 37 °C, 5% CO_2. After incubation, anti-CD4 FITC was added, and the cells were incubated at 4 °C for 30 min in the dark. Fixation was performed using MEDIUM A according to the instructions of the Fix & Rupture Kit (GAS005/2, MultiSciences; Hangzhou, China). After thorough washing, the cells were treated with MEDIUM B and APC-anti-IL-17A and incubated at 4 °C for 1 h. Following another wash, the cells were resuspended in PBS and analyzed by flow cytometry to determine the proportion of $CD4^+$ $IL\text{-}17A^+$ (Th17) cells.

2.14. Quantitative polymerase chain reaction (Q-PCR)

The cells cultivated *in vitro* were subjected to the TRIzol RNA extraction technique to obtain the total RNA, and the suitability of the extracted RNA for further research was confirmed by detecting the optical density (OD) values at wavelengths of 260 and 280 nm. Then, the total RNA was transcribed into complementary DNA (cDNA) with HiScript Q RT SuperMix for qPCR kit (Vazyme; Nanjing, China). Then cDNA was further analyzed using Real-time PCR with the ChamQ universal SYBR qPCR master mix kit (Vazyme; Nanjing, China). The data were calculated using the $2^{-\Delta\Delta Ct}$ method, and primer sequences were provided in Supplementary Table 1.

2.15. Nuclear magnetic resonance (NMR) metabolomics [16]

The cells cultivated *in vitro* were collected and treated with 1 mL of precooled methanolic water and 200 μL chloroform. After 30 min of reaction on ice, the mixture was separated into three different layers by centrifugation. Then, 580 μL of D_2O containing internal standard TMSP (0.05%) was used for further dissolution. After centrifugation at 12 000 r·min^{-1}, the supernatant was carefully transferred to a 5 mm NMR tube and subjected to untargeted metabolite measurements using ^1H NMR spectroscopy at 600 MHz. The spectra were weighted with exponential functions and 0.3 Hz broadening by MestReNova 6.1 software, and data underwent normalization based on the total area, facilitated by the automated software Chenomx NMR Suite 9.02. The main composition and metabolic pathway enrichment analysis were subsequently conducted using MetaboAnalyst 5.0.

2.16. Glucose uptake

The cells were collected and centrifuged at 1200 r·min^{-1} for 5 min at 4 °C, followed by two washes with pre-chilled PBS. They were then subjected to 1 hour of nutrient deprivation using Krebs-Ringer HEPES (KRH) solution. Subsequently, 100 μL of the 2-[*N*-(7-nitrobenz-2-oxa-1,3-diazol-4-yl) amino]-2-deoxy-D-glucose (2-NBDG, 500 μmol·L^{-1}) was added, and the cells were incubated at 37 °C in darkness for 30 min. After incubation, the cells were collected, and mean fluorescence intensity was quantified using flow cytometry analysis.

2.17. Intracellular pH

The cells were collected and washed twice with pre-chilled PBS. They were then incubated at 37 °C for 30 min with 2',7'-bis-(2-carboxyethyl)-5-(and-6)-carboxyfluorescein, acetoxymethyl ester (BCECF-AM) at a final concentration of 5 μmol·L^{-1}. After incubation, the cells were collected, and mean fluorescence intens-

ity was quantified using flow cytometry analysis.

2.18. Molecular docking

To retrieve the crystallographic configuration of the HK2 molecule: 2NZT from the PDB database (http://www.rcsb.org/). Concurrently, the chemical structure of the target compounds (PubChem CID: 72704451) was obtained from the PubChem database (https://pubchem.ncbi.nlm.nih.gov/). The HK2 molecules were preprocessed with QuickPrep and docked using molecular operating environment (MOE) software.

2.19. Transfection

The cells were suspended in a serum-free medium and transfected with a DNA-PEI complex, prepared using the PEI 40K transfection reagent (Servicebio, Wuhan, China) for 12 h.

2.20. Statistical analysis

Data were statistically analyzed using SPSS 23.0. Intergroup comparisons were performed using a one-way ANOVA, and pairwise comparisons were performed using the least significant difference (LSD) *t*-test in the case of homoscedasticity or the Games-Howell test in the case of heteroscedasticity. Differences were considered statistically significant at $P < 0.05$.

3. Results

3.1. AS inhibits AIA in rats

This study investigated the therapeutic effect of AS on AIA in a rat model. The key features of AIA in rats include primary and secondary paw swelling, weight loss, and chronic systemic inflammation with joint pathological changes. The results (Figs. 1A–1C) showed that compared with rats in the normal group, the AIA rats had significant primary and secondary paw swelling from day 14 onwards as well as a gradual loss of body weights. Pharmacological treatment of AS (50, 100 mg·kg^{-1}; i.v. or 200 mg·kg^{-1}; i.g.) from day 14 to 27 significantly alleviated the loss of body weights and inhibited the primary and secondary paw swelling of AIA rats. DEX (0.5 mg·kg^{-1}), the positive drug, displayed a similar promotion. As shown in Fig. 1D, the photographs visually demonstrated the improvement in paw swelling of AIA rats treated with AS and DEX. Furthermore, the AI scores, which were based on the degree of paw swelling, erythema behind the ears, and nodules in the tail, were significantly reduced by AS (50, 100 mg·kg^{-1}; i.v. or 200 mg·kg^{-1}; i.g.) and DEX (0.5 mg·kg^{-1}) (Fig. 1E).

Finally, to firmly prove the inhibitory effect of AS on arthritis, the pathological changes in ankle joints of AIA rats were evaluated using H&E staining. Compared with the rats in the normal group, AIA rats exhibited a severe increase of synovial cells, with varying degrees of inflammatory cell infiltration in synovial tissues. The pannus formation was also observed on the majority of articular cartilage surfaces, and both the articular cartilage and bone tissue showed varying extents of destruction. After administration of AS (50, 100 mg·kg^{-1}; i.v. or 200 mg·kg^{-1}; i.g.) or DEX (0.5 mg·kg^{-1}), the severity of pathological changes was significantly reduced (Figs. 1F and 1G). The relief of bone destruction was visualized with the help of X-rays (Fig. 1H). Furthermore, the inflammatory mediators TNF-α, IL-1β, and IL-6 play important roles in RA pathogenesis, and their levels in serum or joint tissues were obviously down-regulated by AS (50, 100 mg·kg^{-1}; i.v. or 200 mg·kg^{-1}; i.g.) or DEX (0.5 mg·kg^{-1}) (Fig. 1I). These findings demonstrated that AS played a significant role in inhibiting arthritis, protecting synovial tissues, and improving bone destruction of AIA rats.

3.2. AS improves the unbalanced lymphocyte homeostasis

Although the pathogenesis of RA is complex and has not been fully elucidated, the immune cells play important mediating roles. After being stimulated by antigens, CD4$^+$ T cells are activated and differentiated into different subgroups under the action of specific cytokines, maintaining a delicate balance at the level of transcription factors, cytokines, and key genes [17]. In recent years, the imbalance between Th17 and Treg cells has been identified as a key trigger for RA [18]. This study utilized a database to verify the relationship between AS and RA. A total of 3617 RA-related genes were obtained from GeneCards, with 74 overlapping targets between AS and RA, primarily enriched in immune system processes (Fig. 2A). The spleen, a vital immune organ, exhibited a reduced spleen index upon AS administration (50, 100 mg·kg^{-1}; i.v. or 200 mg·kg^{-1}; i.g.), suggesting a potential immunomodulatory effect (Fig. 2B). Then, results of ELISA further indicated that the level of IL-17A, the function-related factor of Th17 cells, in the serum and of AIA rats was significantly reduced by AS (50, 100 mg·kg^{-1}; i.v. or 200 mg·kg^{-1}; i.g.) (Fig. 2C). However, as shown in Fig. 2D, AS also elevated the Treg cell-related factor IL-10 in the serum, but the regulation of AS on IL-17A was more significant. Moreover, the expression level of RORγt, the crucial transcription factor for Th17 cell differentiation, was significantly inhibited by AS in joint tissues (Fig. 2E). These findings suggest that the effect of AS on Th17 cell differentiation warrants further investigation.

3.3. AS significantly inhibits Th17 cell differentiation

Studies have shown a notable increase in the proportion of Th17 cells in both the synovial fluid and peripheral blood of individuals with RA compared to healthy individuals [19]. This elevation is positively correlated with the severity of the disease, emphasizing the critical role of Th17 cells in RA [20]. Before examining the inhibitory effect of AS on Th17 cell differentiation, its toxic effect on CD4$^+$ T cells was initially assessed by quantifying the vitality of lymphocytes using MTT and apoptosis assays. The results in Fig. 3A indicated that AS showed no cytotoxicity at concentrations below 25 μmol·L^{-1}, deeming concentrations of 1.56, 3.125, 6.25, and 12.5 μmol·L^{-1} as safe (Fig. 3A). Subsequently, the cell apoptosis was further showed to be slightly affected by AS (1.56, 3.125, 6.25, 12.5 μmol·L^{-1}) (Fig. 3B). As depicted in Fig. 3C, AS (3.125, 6.25, 12.5 μmol·L^{-1}) treatment led to a decrease in the proportion of CD4$^+$ IL-17A$^+$ T cells (Th17 cells) compared to the Th17 group. The mRNA levels of the Th17 cells-specific transcription factor RORγt, as well as functional factors IL-17A, IL-21, IL-22, and IL-17F, were significantly reduced (Figs. 3D and 3E). Collectively, these findings suggest that AS has the potential to inhibit the differentiation of Th17 cells.

3.4. AS regulates glycolytic metabolism during Th17 cell differentiation

Glycolysis, glutaminolysis, and fatty acid metabolism stand as the primary triumvirate of metabolic pathways facilitating the provision of energy for CD4$^+$ T cells. The orchestration of energy metabolism assumes a pivotal regulatory role in the differentiation of Th17 cells [21]. Consequently, NMR non-targeted metabolomics was employed to assess the impact of AS on the metabolic profile during Th17 cell differentiation. The principal component analysis (PCA), partial least squares-discriminant analysis (PLS-DA), and orthogonal partial least squares-discriminant analysis (OPLS-DA) plots delineated metabolic variations between the Th17 and AS groups (Figs. 4A–4C). The heatmap illustrated the intracellular metabolite differences (Fig. 4D). Notably, AS (12.5 μmol·L^{-1}) exhibited a significant reduction in products such as lactate and pyruvate, suggesting a potential influence on the glycolytic metabolism. The results of KEGG pathway enrichment

analysis observed significant alterations in glycolysis-related pathways (Fig. 4E). Additionally, flow cytometry analysis revealed that AS (12.5 μmol·L^{-1}) significantly decreased the glucose uptake and increased the pH values, corroborating the consistency with the metabolomics results (Figs. 4F and 4G).

3.5. HK2 is involved in AS-mediated limitation on Th17 cell differentiation

The impact of AS on glycolysis during Th17 cell differentiation was further assessed based on the metabolomics findings. Evidence suggests that key rate-limiting enzymes are of utmost importance in the process of glycolysis [22]. Consequently, this study investigated the levels of critical rate-limiting enzymes in glycolysis. As depicted in Fig. 5A, when exposed to Th17-inducing conditions, AS exhibited a reduction in the level of HK2, whereas the protein levels of PKM2 and GAPDH remained unaltered. Molecular docking analysis elucidated that AS successfully integrated into the binding pocket and interacted with the amino acids surrounding the HK2 protein, and the binding free energy was determined to be −6.69 kcal·mol^{-1}. The AS formed multiple hydrogen connections with neighboring amino acid

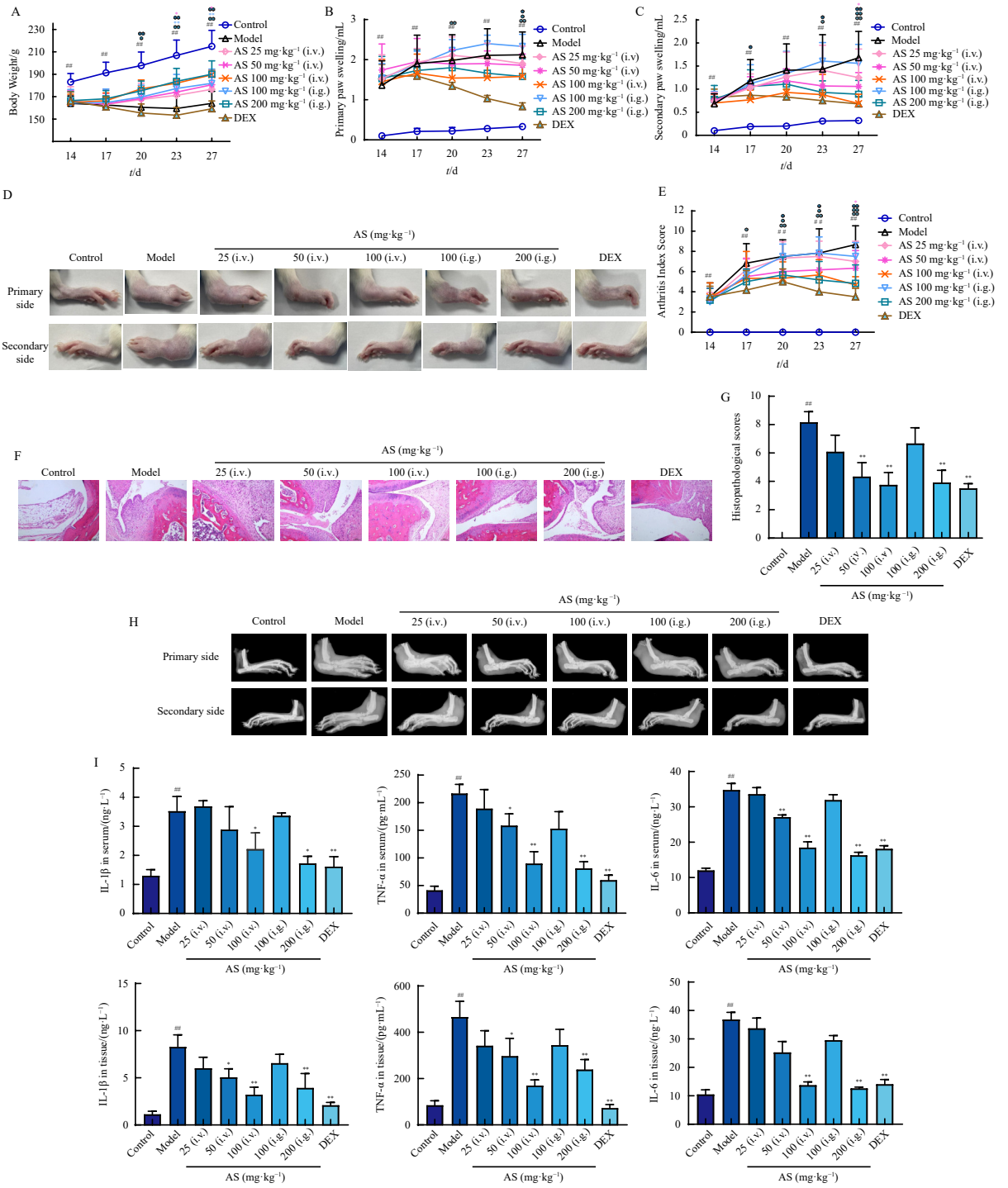

Fig. 1 Effect of andrographolide sulfonate (AS) on adjuvant-induced arthritis (AIA) in rats. The AIA model was established *via* intradermal injection of Freund's complete adjuvant to the right hind paws and tail roots of rats and treated with AS or dexamethasone (DEX) from day 14 to day 27. (A) The body weights. (B, C) The primary and secondary paw swelling. (D) The representative photographs of paws. (E) The AI scores. (F, G) The histopathological changes and quantitative scoring. (H) The X-rays were taken to judge the degree of joint erosion. (I) The levels of TNF-α, IL-1β, and IL-6 in the serum and joint tissues were measured with ELISA kits. Data were expressed as mean ± SEM (n = 6). $^{\#\#}P < 0.01$ *vs* normal group; $^{*}P < 0.05$, $^{**}P < 0.01$ *vs* model group.

residues, such as Arg462 and Gln466 (Fig. 5B). Subsequently, the participation of HK2 in AS-inhibited Th17 cell differentiation was validated through plasmid transfection. As illustrated in Figs. 5C–5E, the overexpression of HK2 mitigated the down-regulation of $CD4^+$ IL-$17A^+$ (Th17 cells) proportion and the levels of IL-17A and RORγt, functional factors of Th17 cell, induced by AS (12.5 μmol·L^{-1}). This substantiates the involvement of HK2-mediated glycolysis in the inhibition of Th17 cell differentiation by AS.

3.6. The PI3K/AKT pathway plays a crucial role in AS-inhibited Th17 cell differentiation following glycolysis disruption

The PI3K/AKT pathway plays a crucial role in regulating cell proliferation, survival, and differentiation, thereby impacting the development and progression of diseases [23]. Notably, increased glycolytic activity leads to excessive AKT activation [24]. To investigate the potential anti-RA mechanisms of AS, a PPI network was constructed based on AS targets, identifying 20 key hub genes, with AKT ranking among the top five targets (Fig. 6A). As illustrated in Fig. 6B, AS (12.5 μmol·L^{-1}) significantly reduced the levels of p-AKT and p-PI3K under the Th17-inducing conditions. Similar results were observed *in vivo*, whereas AS (50, 100 mg·kg^{-1}; *i.v.* or 200 mg·kg^{-1}; *i.g.*) alleviated AKT and PI3K phosphorylation in AIA rats (Fig. 6C). As expected, the exogenous addition of the glycolysis product lactate (2 mmol·L^{-1}), but not pyruvate (2 mmol·L^{-1}), obviously reversed the AS-induced suppression of AKT and PI3K activation in Th17 cell differentiation (Fig. 6D). Further investigations demonstrated that AS (12.5 μmol·L^{-1}) downregulated Th17 cell proportions, RORγt expression, and IL-17A levels (Fig. 6E–6I). Collectively, these findings suggest that AS inhibits Th17 cell differentiation by impairing PI3K/AKT pathway activation through glycolysis suppression.

4. Discussion

The molecular mechanisms underlying RA are extremely complex and have not yet been fully elucidated. Over the last two decades, new therapeutic regimens involving the use of selective antagonistic inflammatory cytokines have been developed for the clinical treatment of RA, including the TNF-α inhibitors (infliximab, certolizumab, and adalimumab), the IL-1 receptor inhibitor (anakinra), and IL-6 inhibitors (sarilumab and tocilizumab) [25-27]. However, the utilization of multiple drugs may increase safety risks and financial burdens on patients. The AIA model in rats exhibits similarities to human RA in clinical features and pathological characteristics, making it a classical tool for the study and development of anti-RA therapies [28, 29]. In the present study, experimental verification was performed by using the AIA model in rats, and a well-documented alleviation of AS was confirmed by detecting the body weights, paw swelling, AI scores, histopathological changes of ankle joints, as well as the levels of inflammation-related cytokines.

T cells play a crucial role in the adaptive immune response to RA. After antigenic stimulation, $CD4^+$ T cells are activated and dif-

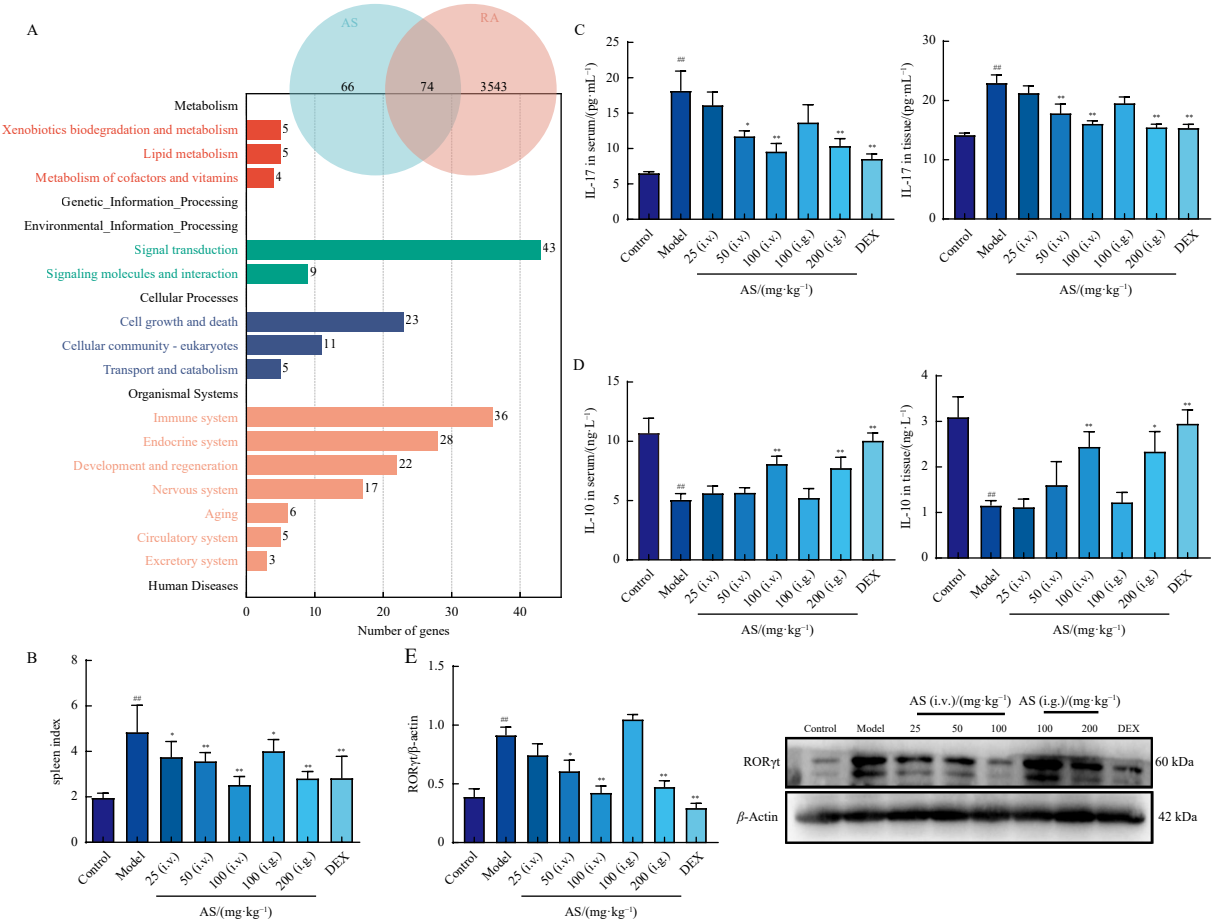

Fig. 2 Effect of andrographolide sulfonate (AS) on the unbalanced lymphocyte homeostasis. (A) The relationship of AS and rheumatoid arthritis (RA). One hundred and forty predicted targets for AS (in the blue circle) were mapped to 3617 RA-related targets in the GeneCards database (in the pink circle). The intersection of these targets resulted in the identification of 74 potential anti-RA targets of AS, and these targets were used for KEGG pathway annotation. (B–E) The adjuvant-induced arthritis (AIA) model was established *via* intradermal injection of Freund's complete adjuvant to the right hind paws and tail roots of rats and treated with AS or dexamethasone (DEX) from day 14 to day 27. Then, the spleens were collected, and splenic indexes were calculated (B). The levels of IL-10 and IL-17 in the serum and joint tissues were measured with ELISA kits (C, D). The relative levels of RORγt were analyzed using Western blotting assay (E). Data were expressed as mean ± SEM (n = 6). $^{\#\#}P < 0.01$ *vs* normal group; $^{*}P < 0.05$, $^{**}P < 0.01$ *vs* model group.

ferentiate into different subtypes, including Th1, Th2, Th17, and Treg cells, under the action of specific cytokines [30, 31]. These subsets interact at the transcriptional, cytokine, and genetic levels to maintain a delicate balance, the disruption of which can lead to immune disorders. The traditional view has been that RA is caused by a Th1/Th2 imbalance. However, recent studies suggest that a Th17/Treg imbalance may be a significant factor. Th17 cells activate synovial fibroblasts and macrophages to produce inflammatory factors, inducing synovial inflammation through the secretion of IL-17A [32, 33]. Th17 cells can also promote osteoclast formation, leading to cartilage destruction and bone erosion. Treg cells are immunosuppressive and can antagonize the function of Th17 cells by secreting the anti-inflammatory cytokine IL-10 [34]. An imbalance in IL-17/IL-10 levels may contribute to immune dysregulation in RA patients [35]. The present study demonstrated that the levels of IL-17 in the serum and joint tissues of AIA rats were significantly reduced by AS, while IL-10 levels were significantly upregulated. Furthermore, the *in vitro* model of Th17 differentiation confirmed the inhibitory effects of AS.

The initial CD4$^+$ T cells are mainly powered by fatty acid oxidation and oxidative phosphorylation following the entry of pyruvate into the mitochondria. Under the influence of antigen stimulation, they are rapidly activated and proliferated. They then differentiate into Th17 or Treg cells in response to specific cytokines [24, 36]. Gerriets VA et al. studied 400 energy metabolites in Th17 and Treg cells using liquid chromatography/gas chromatography-mass spectrometry (LC/GC-MS) and found distinct metabolic characteristics [37]. Th17 cells exhibit high levels of pyruvate and lactic acid, while Treg cells have more tricarboxylic acid cycle (TCA) cycle intermediates, indicating that Th17 cells predominantly rely on glycolysis for energy supply, whereas Treg cells primarily depend on pyruvate oxidative phosphorylation and

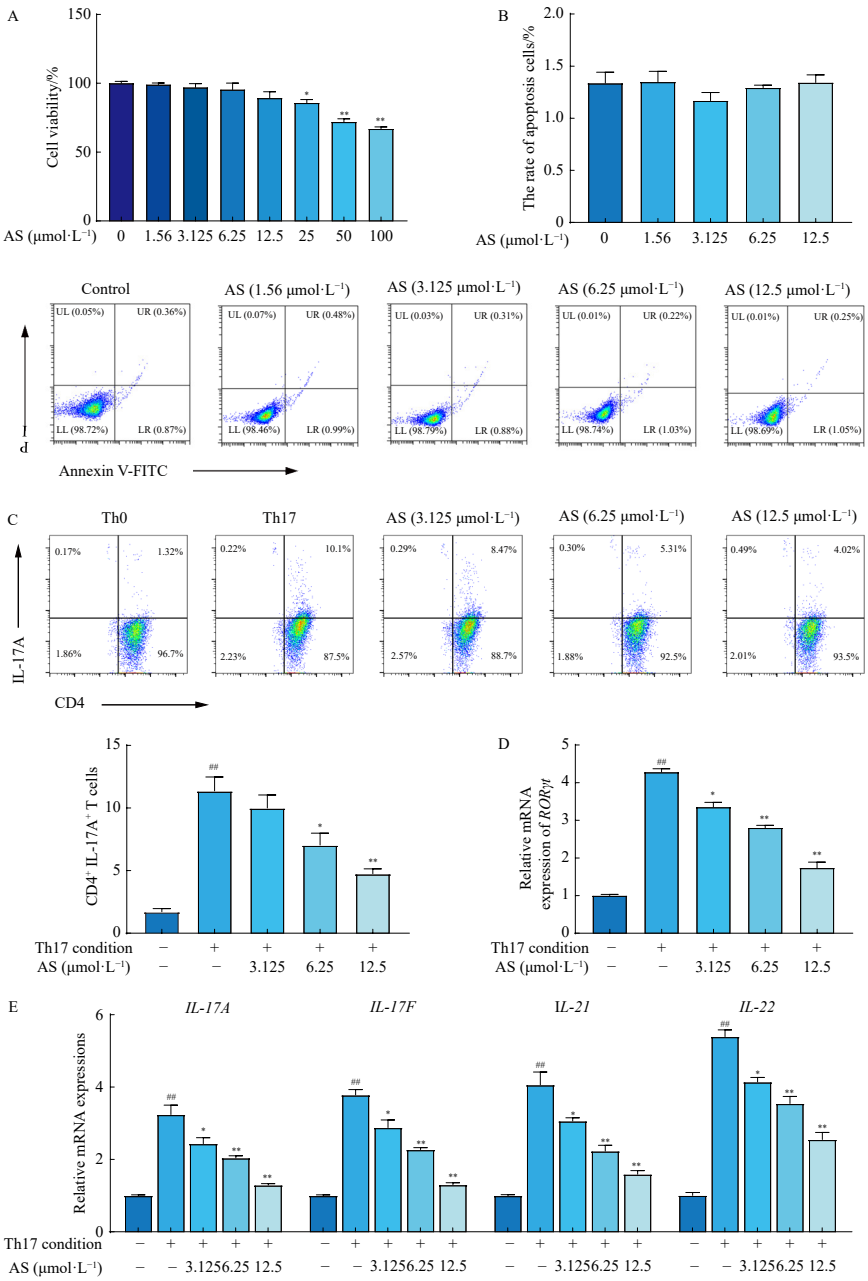

Fig. 3 Effect of andrographolide sulfonate (AS) on the differentiation of Th17 cells. The CD4$^+$ T cells were treated with AS (1.56, 3.125, 6.25, 12.5, 25, 50, 100 μmol·L^{-1}) for 72 h, and the cell viability was detected using MTT assay (A). In addition, the cell apoptosis was also determined in the presence of AS (1.56, 3.125, 6.25, 12.5 μmol·L^{-1}) using the Annexin V-FITC apoptosis kit (B). (C, D) The CD4$^+$ T cells were differentiated under Th17-inducing conditions for 3 d in the presence or absence of AS (3.125, 6.25, 12.5 μmol·L^{-1}). The proportions of CD4$^+$ IL-17$^+$ T cells (C) and the relative mRNA expressions of *RORγt* (D), *IL-17A*, *IL-17F*, *IL-21* and *IL-22* (E) were examined by flow cytometry or Q-PCR. Data were presented as the means ± SEM of three independent experiments. $^{\#}P < 0.05$, $^{\#\#}P < 0.01$ *vs* Th0 group; $^{*}P < 0.05$, $^{**}P < 0.01$ *vs* Th17 group.

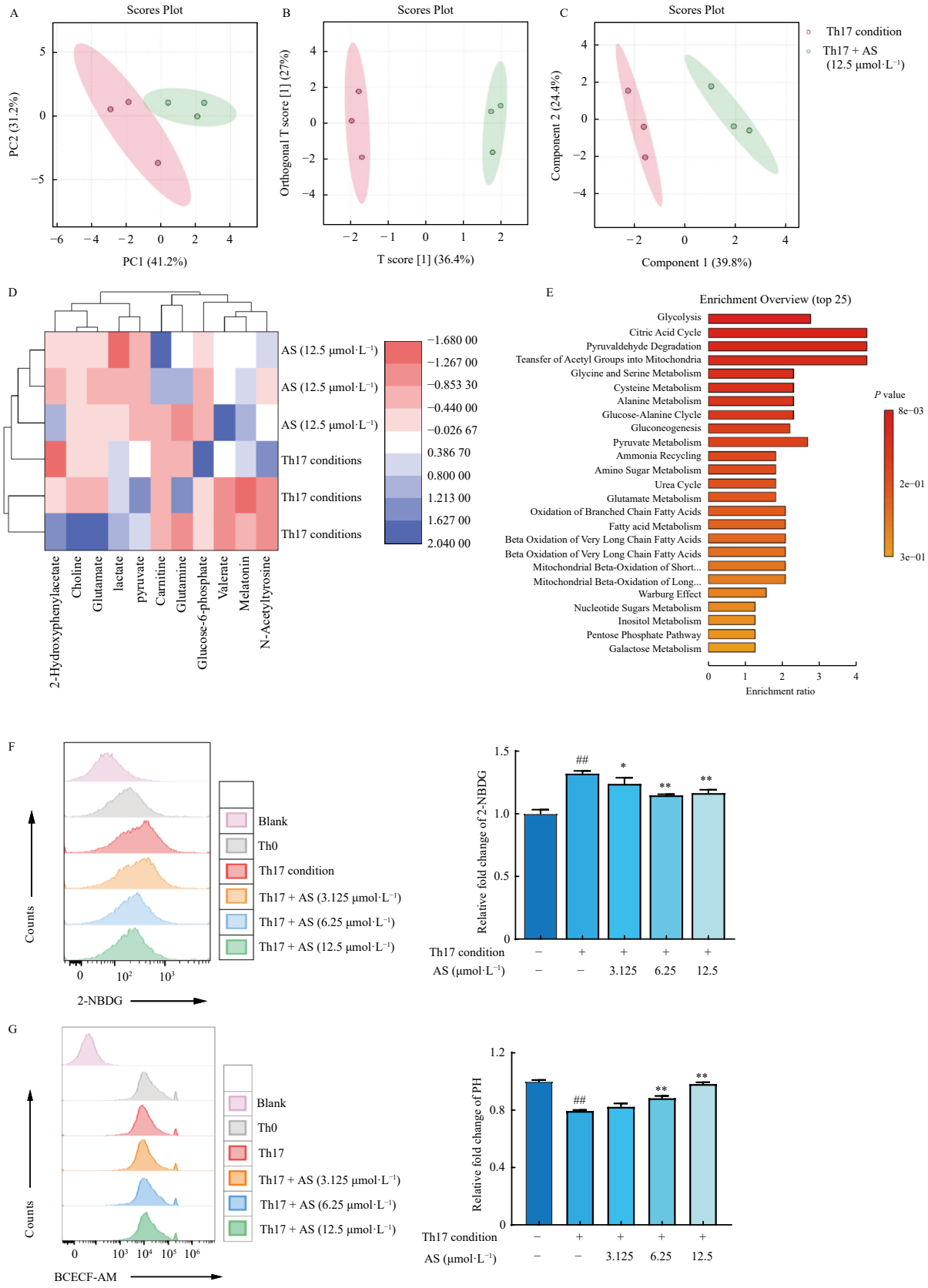

Fig. 4 The impact of andrographolide sulfonate (AS) on the metabolic profile of Th17 cells. (A–E) The lysates of Th17 cells with or without AS (12.5 μmol·L^{-1}) were extracted and analyzed using NMR for the determination of cellular metabolites. (A–C) The PCA, PLS-DA, and OPLS-DA plots were presented. The heatmap (D) and metabolic pathway enrichment (E) analysis were shown based on the relative abundance of metabolites. (F, G) The CD4$^+$ T cells were differentiated under Th17-inducing conditions for 72 h in the presence or absence of AS (3.125, 6.25, 12.5 μmol·L^{-1}). The relative glucose uptake (F) and intracellular pH values (G) were determined using flow cytometry to detect the fluorescence intensity of 2-NBDG or BCECF-AM. Data were presented as the means ± SEM of three independent experiments. $^{\#}P < 0.05$, $^{\#\#}P < 0.01$ *vs* Th0 group; $^{*}P < 0.05$, $^{**}P < 0.01$ *vs* Th17 group.

fatty acid oxidative decomposition for energy supply [38]. Gene expression data shows similar results, with glucose metabolism-related genes, such as HK2, being more highly expressed in Th17 cells, while genes related to fatty acid metabolism, such as carnitine palmitoyl transferase I (CPT1), are more highly expressed in Treg cells [39, 40]. Non-targeted metabolomics and KEGG pathway enrichment analysis in this study highlighted the crucial role of glycolysis as the main regulatory metabolic pathway following AS treatment, a finding further validated by the observed glucose uptake and alterations in pH levels.

Glycolysis is a metabolic cascade that occurs in the cytoplasm, converting glucose into pyruvate. Glucose typically enters the cytoplasm from the external environment, facilitated by glucose transporters. Once inside, it is transformed into glucose 6-phosphate by HKs, and glyceraldehyde 3-phosphate undergoes oxidation catalyzed by GAPDH to produce 1,3-diphosphoglycerate after a multi-step reaction. Additionally, PKMs catalyze the conversion of phosphoenolpyruvate to pyruvate, which is then transported into the mitochondria to undergo the tricarboxylic acid cycle [41, 42]. Studies report that HK2 inhibitors, such as 2-deoxy-D-glucose (2-DG) and 3'-bromopyruvate, promote the differentiation of regulatory T (Treg) cells by blocking the glycolytic pathway and inhibiting Th17 cell differentiation, significantly improving experimental autoimmune encephalomyelitis in mice induced by myelin oligodendrocyte glycoprotein$_{35-55}$ [43, 44]. It is well-established that PKM2 is an important mediator in controlling Th17 differentiation, but the determining factors of Th17 cell transformation remain unclear. The findings of this study demonstrated that AS significantly reduced the level of HK2, but not PKM2 or GAPDH, during Th17 cell differentiation. As expec-

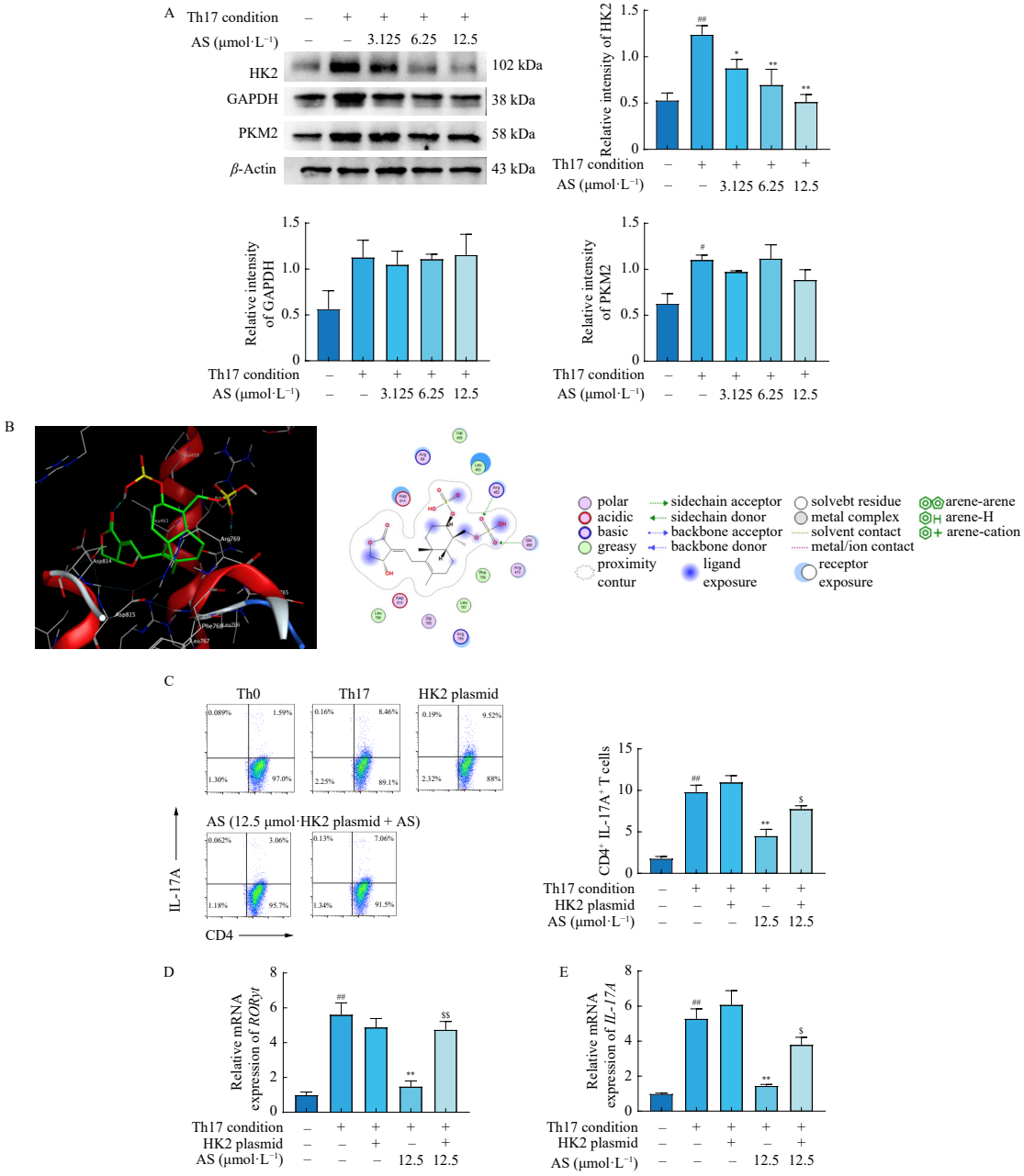

Fig. 5 The key rate-limiting enzymes that are responsible for andrographolide sulfonate (AS) to resist glycolysis. (A) The CD4$^+$ T cells were differentiated under Th17-inducing conditions for 72 h in the presence or absence of AS (3.125, 6.25, 12.5 μmol·L^{-1}). The glycolysis-related glucose transporter or metabolic enzymes were detected using Western blotting assay. (B) The association of AS and HK2 was simulated using molecular docking. (C, D) The CD4$^+$ T cells were differentiated under Th17-inducing conditions for 72 h in the presence or absence of HK2 overexpression plasmid and AS (12.5 μmol·L^{-1}). The proportions of IL-17$^+$ T cells were gated by flow cytometry (C). The mRNA levels of *RORγt* and *IL-17A* were detected using Q-PCR (D, E). Data were presented as the means ± SEM of three independent experiments. $^{\#}P < 0.05$, $^{\#\#}P < 0.01$ *vs* Th0 group; $^{*}P < 0.05$, $^{**}P < 0.01$ *vs* Th17 group; $^{\$}P < 0.05$, $^{\$\$}P < 0.01$ *vs* HK2 overexpression plasmid group.

ted, overexpression of HK2 abolished the inhibitory effect of AS on Th17 cells.

The precise mechanisms by which glycolysis regulates the impact of AS on the differentiation of Th17 cells remain unclear. However, bioinformatics analysis has revealed that the PI3K/Akt signaling pathway is a potential target for the effects of AS on RA. *In vivo* and *in vitro* experimental data demonstrate that AS significantly downregulates the phosphorylation of PI3K and AKT in the joints of AIA rats and in $CD4^+$ T cells under Th17-inducing conditions. Notably, an acidic environment regulated by ornithine decarboxylase 1 can control the activation of AKT, which affects the proliferation, invasion, and migration of hepatocellular carcinoma cells [45]. Additionally, 2-DG has been reported to prevent the activation of AKT in lung cancer cells [46]. In osteoarthritis, the metabolite lactate upregulates NADPH oxidase by activating the PI3K/AKT signaling pathway through the receptor hydroxycarboxylic acid receptor 1 (HCAR1) [47, 48]. The addition of lactate under Th17-inducing conditions reversed the inhibitory effects of AS on the PI3K/AKT pathway, and when lactate was supplemented, AS was unable to disrupt the differentiation of Th17 cells.

While andrographolide has been reported to exert anti-RA effects and mitigate hepatic damage caused by methotrexate [49], studies have also indicated that different derivatives of andrographolide can have varying activities and toxicity due to changes in functional groups and structure [50, 51]. The derivatization of andrographolide into AS involved the addition of sulfonic acid substituent groups and the rearrangement of double bonds, resulting in enhanced water solubility, but it may also lead to changes in biological activities. Therefore, investigations are required to determine whether AS possesses anti-RA properties. This study

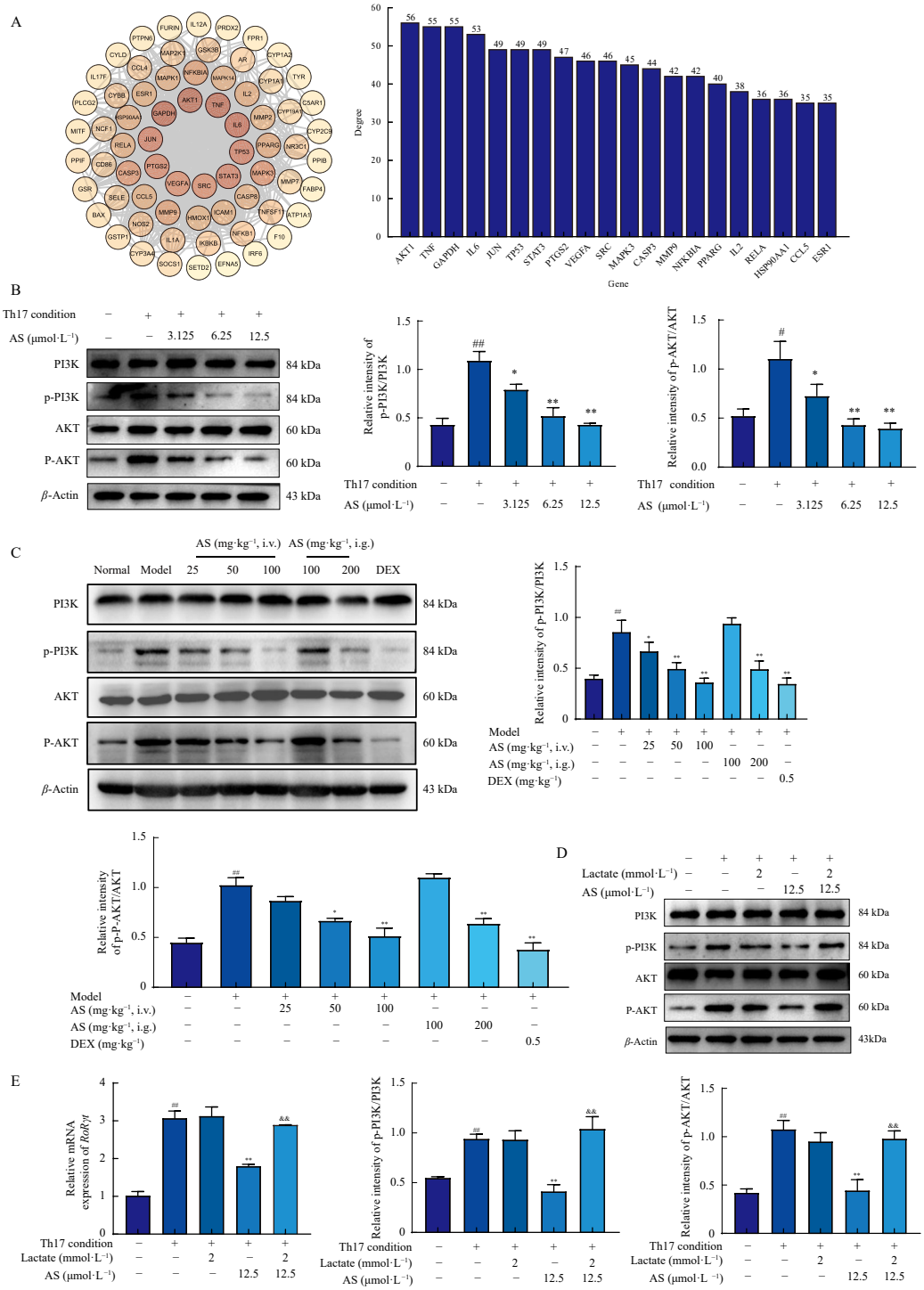

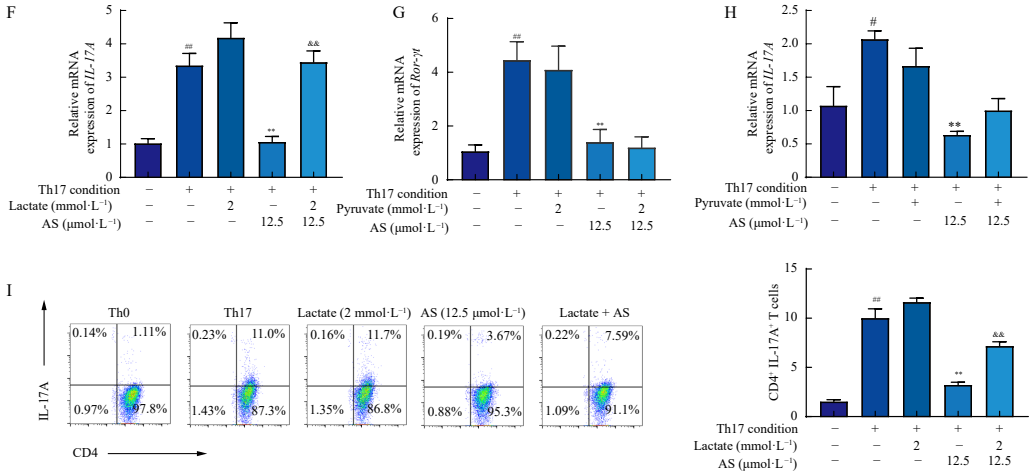

Fig. 6 Andrographolide sulfonate (AS) alleviates the activation of PI3K/AKT to repress Th17 cell differentiation after inhibiting glycolysis. (A) Hub gene identification. PPI network of the potential anti-RA targets of AS (the transition from yellow to red signifies the association from minimal to maximal connectivity degree), the 20 hub genes from the whole PPI network were identified using the Cytohubba plugin in Cytoscape and were ordered by degree. (B) The $CD4^+$ T cells were differentiated under Th17-inducing conditions for 72 h in the presence or absence of AS (3.125, 6.25, 12.5 μmol·L^{-1}). The phosphorylation levels of PI3K and AKT were detected using Western blotting assay. (C) The adjuvant-induced arthritis (AIA) model was established *via* intradermal injection of Freund's complete adjuvant to the right hind paws and tail roots of rats and treated with AS or dexamethasone (DEX) from day 14 to day 27. The phosphorylation levels of PI3K and AKT in ankle joints were detected using Western blotting assay. (D–H) The $CD4^+$ T cells were differentiated under Th17-inducing conditions for 72 h in the presence or absence of lactate (2 mmol·L^{-1}) or pyruvate (2 mmol·L^{-1}) and AS (12.5 μmol·L^{-1}). The phosphorylation levels of PI3K and AKT were detected using Western blotting assay (D). The mRNA expressions of RORγt (E, G) and IL-17A (F, H) were detected using Q-PCR. (I) The $CD4^+$ T cells were differentiated under Th17-inducing conditions for 72 h in the presence or absence of lactate (2 mmol·L^{-1}) and AS (12.5 μmol·L^{-1}). The proportions of $IL\text{-}17^+$ T cells were gated by flow cytometry (I). Data were presented as the means ± SEM of six rats or three independent experiments. $^{\#}P < 0.05$, $^{\#\#}P < 0.01$ *vs.* normal or Th0 group; $^{*}P < 0.05$, $^{**}P < 0.01$ *vs.* model or Th17 group; $^{\&}P < 0.05$, $^{\&\&}P < 0.01$ *vs.* AS group.

has provided the research data to support the use of AS in treating RA for the first time. Notably, AS has already been approved for the clinical treatment of other inflammation-related diseases, and its safety has been validated by a considerable amount of clinical data [52]. These factors suggest that AS may potentially serve as a safe and effective therapeutic drug for the treatment of RA, which will broaden its potential application and repurposing investigations.

5. Conclusion

The findings of this study revealed that AS produced substantial therapeutic benefits in the AIA rat model. These effects included increased body weight, significant inhibition of primary and secondary paw swelling, reduced arthritic index and splenic index scores, as well as improved joint injury and pathological changes within the tissue in a dose- and time-dependent manner. The potential mechanisms underlying these therapeutic effects may be attributed to the inhibited differentiation of Th17 cells *via* the glycolysis-controlled activation of the PI3K/AKT pathway.

Funding

This work was supported by the project of Central Funds Guiding the Local Science and Technology Development (No. 20212ZDD02010).

Declaration of competing interest

These authors have no conflict of interest to declare.

Acknowledgements

We thank Shanghai NewCore Biotechnology Co., Ltd. (https://www.bioinformatics.com.cn) for providing an online visualization platform.

References

1 Smith MH, Berman JR. What is rheumatoid arthritis? *JAMA*. 2022;327(12):1194. https://doi.org/10.1001/jama.2022.0786.
2 Pirmardvand Chegini S, Varshosaz J, Taymouri S. Recent approaches for targeted drug delivery in rheumatoid arthritis diagnosis and treatment. *Artif Cells Nanomed Biotechnol*. 2018;46(sup2):502-514. https://doi.org/10.1080/21691401.2018.1460373.
3 Smolen JS, Aletaha D, McInnes IB. Rheumatoid arthritis. *Lancet*. 2016;388(10055):2023-2038. https://doi.org/10.1016/S0140-6736(16)30173-8.
4 Myasoedova E. New era for outcomes and management of rheumatoid arthritis: facing the individualized treatment challenge. *Joint Bone Spine*. 2021;88(3):105066. https://doi.org/10.1016/j.jbspin.2020.08.001.
5 Zingler G, Hermann B, Fischer T, et al. Cardiovascular adverse events by non-steroidal anti-inflammatory drugs: when the benefits outweigh the risks. *Expert Rev Clin Pharmacol*. 2016;9(11):1479-1492. https://doi.org/10.1080/17512433.2016.1230495.
6 Radu AF, Bungau SG. Management of rheumatoid arthritis: an overview. *Cells*. 2021;10(11):2857. https://doi.org/10.3390/cells10112857.
7 Hyndman IJ. Rheumatoid arthritis: past, present and future approaches to treating the disease. *Int J Rheum Dis*. 2017;20(4):417-419. https://doi.org/10.1111/1756-185X.12823.
8 Kumar S, Singh B, Bajpai V. *Andrographis paniculata* (Burm. f.) nees: traditional uses, phytochemistry, pharmacological properties and quality control/quality assurance. *J Ethnopharmacol*. 2021;275:114054. https://doi.org/10.1016/j.jep.2021.114054.
9 Yen CC, Chen YC, Wu MT, et al. Nanoemulsion as a strategy for improving the oral bioavailability and anti-inflammatory activity of andrographolide. *Int J Nanomed*. 2018;13:699-680. https://doi.org/10.2147/IJN.S154824.
10 Guo W, Liu W, Chen G, et al. Water-soluble andrographolide sulfonate exerts anti-sepsis action in mice through down-regulating p38 MAPK, STAT3 and NF-κB pathways. *Int Immunopharmacol*. 2012;14(4):613-619. https://doi.org/10.1016/j.intimp.2012.09.002.
11 Gao J, Cui J, Zhong H, et al. Andrographolide sulfonate ameliorates chronic colitis induced by TNBS in mice *via* decreasing inflammation and fibrosis. *Int Immunopharmacol*. 2020;83:106426. https://doi.org/10.1016/j.intimp.2020.106426.
12 Pan R, Dai Y, Gao X, et al. Scopolin isolated from *Erycibe obtusifolia* Benth stems suppresses adjuvant-induced rat arthritis by inhibiting inflammation and angiogenesis. *Int Immunopharmacol*. 2009;9(7-8):859-869. https://doi.org/10.1016/j.intimp.2009.02.019.
13 Jawed H, Shah SU, Jamall S, et al. *N*-(2-hydroxy phenyl) acetamide inhibits inflammation-related cytokines and ROS in adjuvant-induced arthritic (AIA) rats. *Int Immunopharmacol*. 2010;10(8):900-905. https://doi.org/10.1016/j.intimp.2010.04.028.
14 Yue M, Tao Y, Fang Y, et al. The gut microbiota modulator berberine ameliorates collagen-induced arthritis in rats by facilitating the generation of butyrate and adjusting the intestinal hypoxia and nitrate supply. *FASEB J*. 2019;33(11):12311-12323. https://doi.org/10.1096/fj.201900425RR.
15 Guo F, Jiang C, Xi Y, et al. Investigation of pharmacological mechanism of natural product using pathway fingerprints similarity based on "drug-target-pathway" heterogenous network. *J Cheminform*. 2021;13(1):68. https://doi.org/10.1186/s13321-021-00549-5.
16 Xue X, Zeng X, Wu X, et al. SIRT4 protects against intestinal fibrosis by facilitating GLS1 degradation. *Matrix Biol*. 2023;122:33-45. https://doi.org/10.1016/j.matbio.2023.08.001.
17 Jang S, Kwon EJ, Lee JJ. Rheumatoid arthritis: pathogenic roles of diverse immune cells. *Int J Mol Sci*. 2022;23(2):905. https://doi.org/10.3390/ijms23020905.
18 Jin S, Chen H, Li Y, et al. Maresin 1 improves the Treg/Th17 imbalance in

rheumatoid arthritis through miR-21. *Ann Rheum Dis*. 2018;77(11):1644-1652. https://doi.org/10.1136/annrheumdis-2018-213511.
19 Yang P, Zhang M, Wang X, et al. MicroRNA let-7g-5p alleviates murine collagen-induced arthritis by inhibiting . *Biochem Pharmacol*. 2020;174:113822. https://doi.org/10.1016/j.bcp.2020.113822.
20 Toghi M, Bitarafan S, Ghafouri-Fard S. Pathogenic Th17 cells in autoimmunity with regard to rheumatoid arthritis. *Pathol Res Pract*. 2023;250:154818. https://doi.org/10.1016/j.prp.2023.154818.
21 Peng HY, Lucavs J, Ballard D, et al. Metabolic reprogramming and reactive oxygen species in T cell immunity. *Front Immunol*. 2021;12:652687. https://doi.org/10.3389/fimmu.2021.652687.
22 Bian X, Jiang H, Meng Y, et al. Regulation of gene expression by glycolytic and gluconeogenic enzymes. *Trends Cell Biol*. 2022;32(9):786-799. https://doi.org/10.1016/j.tcb.2022.02.003.
23 Fu S, Song X, Hu Y, et al. Neotuberostemonine and tuberostemonine ameliorate pulmonary fibrosis through suppressing TGF-β and SDF-1 secreted by macrophages and fibroblasts *via* the PI3K-dependent AKT and ERK pathways. *Chin J Nat Med*. 2023;21(7):527-539. https://doi.org/10.1016/s1875-5364(23)60444-3.
24 Woo YM, Shin Y, Lee EJ, et al. Inhibition of aerobic glycolysis represses Akt/mTOR/HIF-1α axis and restores tamoxifen sensitivity in antiestrogen-resistant breast cancer cells. *PLoS One*. 2015;10(7):e0132285. https://doi.org/10.1371/journal.pone.0132285.
25 Feldmann M, Maini SR. Role of cytokines in rheumatoid arthritis: an education in pathophysiology and therapeutics. *Immunol Rev*. 2008;223:7-19. https://doi.org/10.1111/j.1600-065X.2008.00626.x.
26 Kohler BM, Gunther J, Kaudewitz D, et al. Current therapeutic options in the treatment of rheumatoid arthritis. *J Clin Med*. 2019;8(7):938. https://doi.org/10.3390/jcm8070938.
27 Mateen S, Zafar A, Moin S, et al. Understanding the role of cytokines in the pathogenesis of rheumatoid arthritis. *Clin Chim Acta*. 2016;455:161-171. https://doi.org/10.1016/j.cca.2016.02.010.
28 Pan H, Guo R, Ju Y, et al. A single bacterium restores the microbiome dysbiosis to protect bones from destruction in a rat model of rheumatoid arthritis. *Microbiome*. 2019;7(1):107. https://doi.org/10.1186/s40168-019-0719-1.
29 Shao X, Zhang H, Rajian JR, et al. ^{125}I-labeled gold nanorods for targeted imaging of inflammation. *ACS Nano*. 2011;5(11):8967-8973. https://doi.org/10.1021/nn203138t.
30 Jiang Y, Wang X, Dong C. Molecular mechanisms of T helper 17 cell differentiation: emerging roles for transcription cofactors. *Adv Immunol*. 2019;144:121-153. https://doi.org/10.1016/bs.ai.2019.09.003.
31 Ruterbusch M, Pruner KB, Shehata L, et al. *In vivo* CD4$^+$ T cell differentiation and function: revisiting the Th1/Th2 paradigm. *Annu Rev Immunol*. 2020;38:705-725. https://doi.org/10.1146/annurev-immunol-103019-085803.
32 Boissier MC, Assier E, Falgarone G, et al. Shifting the imbalance from Th1/Th2 to Th17/treg: the changing rheumatoid arthritis paradigm. *Joint Bone Spine*. 2008;75(4):373-375. https://doi.org/10.1016/j.jbspin.2008.04.005.
33 Paradowska-Gorycka A, Wajda A, Romanowska-Próchnicka K, et al. Th17/Treg-related transcriptional factor expression and cytokine profile in patients with rheumatoid arthritis. *Front Immunol*. 2020;11:572858. https://doi.org/10.3389/fimmu.2020.572858.
34 Hui W, Yu D, Cao Z, et al. Butyrate inhibit collagen-induced arthritis *via* Treg/IL-10/Th17 axis. *Int Immunopharmacol*. 2019;68:226-233. https://doi.org/10.1016/j.intimp.2019.01.018.
35 Qiu J, Lu C, Zhang L, et al. Osteoporosis in patients with rheumatoid arthritis is associated with serum immune regulatory cellular factors. *Clin Rheumatol*. 2022;41(9):2685-2693. https://doi.org/10.1007/s10067-022-06212-0.
36 Geltink RIK, Kyle RL, Pearce EL. Unraveling the complex interplay between T cell metabolism and function. *Annu Rev Immunol*. 2018;36:461-488. https://doi.org/10.1146/annurev-immunol-042617-053019.
37 Gerriets VA, Kishton RJ, Nichols AG, et al. Metabolic programming and PDHK1 control CD4$^+$ T cell subsets and inflammation. *J Clin Invest*. 2015;125(1):194-207. https://doi.org/10.1172/JCI76012.
38 Zhang S, Gang X, Yang S, et al. The alterations in and the role of the Th17/Treg balance in metabolic diseases. *Front Immunol*. 2021;12:678355. https://doi.org/10.3389/fimmu.2021.678355.
39 Kidani Y, Bensinger SJ. Reviewing the impact of lipid synthetic flux on Th17 function. *Curr Opin Immunol*. 2017;46:121-126. https://doi.org/10.1016/j.coi.2017.03.012.
40 Zhao L, Wu Q, Wang X, et al. Reversal of abnormal CD4$^+$ T cell metabolism alleviates thyroiditis by deactivating the mTOR/HIF1a/glycolysis pathway. *Front Endocrinol (Lausanne)*. 2021;12:659738. https://doi.org/10.3389/fendo.2021.659738.
41 Bommer GT, Van Schaftingen E, Veiga-da-Cunha M. Metabolite repair enzymes control metabolic damage in glycolysis. *Trends Biochem Sci*. 2020;45(3):228-243. https://doi.org/10.1016/j.tibs.2019.07.004.
42 Liu S, Liao S, Liang L, et al. The relationship between CD4$^+$ T cell glycolysis and their functions. *Trends Endocrinol Metab*. 2023;34(6):345-360. https://doi.org/10.1016/j.tem.2023.03.006.
43 Okano T, Saegusa J, Nishimura K, et al. 3-Bromopyruvate ameliorate autoimmune arthritis by modulating Th17/Treg cell differentiation and suppressing dendritic cell activation. *Sci Rep*. 2017;7:42412. https://doi.org/10.1038/srep42412.
44 Shi LZ, Wang R, Huang G, et al. HIF1alpha-dependent glycolytic pathway orchestrates a metabolic checkpoint for the differentiation of TH17 and Treg cells. *J Exp Med*. 2011;208(7):1367-1376. https://doi.org/10.1084/jem.20110278.
45 Ye Z, Zeng Z, Shen Y, et al. ODC1 promotes proliferation and mobility via the AKT/GSKβ/β-catenin pathway and modulation of acidotic microenvironment in human hepatocellular carcinoma. *Onco Targets Ther*. 2019;12:4081-92. https://doi.org/10.2147/OTT.S198341.
46 BEN-SAHRA I, DIRAT B, LAURENT K, et al. Sestrin2 integrates Akt and mTOR signaling to protect cells against energetic stress-induced death. *Cell Death Differ*. 2013;20(4):611-9. https://doi.org/10.1038/cdd.2012.157.
47 Huang YF, Wang G, Ding L, et al. Lactate-upregulated NADPH-dependent NOX4 expression *via* HCAR1/PI3K pathway contributes to ROS-induced osteoarthritis chondrocyte damage. *Redox Biol*. 2023;67:102867. https://doi.org/10.1016/j.redox.2023.102867.
48 Yang J, Dong C, Wu J, et al. Fructose utilization enhanced by GLUT5 promotes lung cancer cell migration *via* activating glycolysis/AKT pathway. *Clin Transl Oncol*. 2023;25(4):1080-1090. https://doi.org/10.1007/s12094-022-03015-2.
49 Luo SS, Li FF, Xie XQ, et al. Anti-inflammatory and hepatoprotective effects of andrographolide combined with methotrexate on rheumatoid arthritis rats. *J Zhengzhou Univ*. 2020;55:472-475. https://doi.org/10.13705/j.issn.1671-6825.2019.07.074.
50 Dey SK, Bose D, Hazra, A, et al. Cytotoxic activity and apoptosis-inducing potential of di-spiropyrrolidino and di-spiropyrrolizidino oxindole andrographolide derivatives . *PLoS One*. 2013;8(3):e58055. https://doi.org/10.1371/journal.pone.0058055.
51 Toppo E, Darvin SS, Esakkimuthu S, et al. Effect of two andrographolide derivatives on cellular and rodent models of non-alcoholic fatty liver disease. *Biomed Pharmacother*. 2017;95:402-411. https://doi.org/10.1016/j.biopha.2017.08.071.
52 Zhao Y, Huang P, Chen Z, et al. Clinical application analysis of andrographolide total ester sulfonate injection, a traditional Chinese medicine licensed in China. *J Huazhong Univ Sci Technolog (Med Sci)*. 2017;37(2):293-299. https://doi.org/CNKI:SUN:TJYW.0.2017-02-022.